

Numerical Simulation Experiment of Land Surface Physical Processes and Local Climate Effect in Forest Underlying Surface*

LIU Shuhua[†] (刘树华), PAN Ying (潘英), DENG Yi (邓毅), MA Mingmin (马明敏),
JIANG Haimei (姜海梅), LIN Hongtao (蔺洪涛), JIANG Haoyu (蒋浩宇),
LIANG Fuming (梁福明), LIU Heping (刘和平), and WANG Jianhua (王建华)

*Group of Atmospheric Boundary Layer and Turbulence, Ministry Laboratory of Storm and Drought Flood Damage,
Department of Atmospheric Sciences, the School of Physics of Peking University, Beijing 100871*

(Received October 10, 2005)

ABSTRACT

Based on the basic principles of atmospheric boundary layer and plant canopy micrometeorology, a forest underlying surface land surface physical process model and a two-dimensional atmospheric boundary layer numerical model are developed and numerical simulation experiments of biosphere and physiological processes of vegetation and soil volumetric water content have been done on land surface processes with local climate effect. The numerical simulation results are in good agreement with realistic observations, which can be used to obtain reasonable simulations for diurnal variations of canopy temperature, air temperature in canopy, ground surface temperature, and temporal and spatial distributions of potential temperature and vertical wind velocity as well as relative humidity and turbulence exchange coefficient over non-homogeneous underlying surfaces. It indicates that the model developed can be used to study the interaction between land surface process and atmospheric boundary layer over various underlying surfaces and can be extended to local climate studies. This work will settle a solid foundation for coupling climate models with the biosphere.

Key words: forest underlying surface, land surface physical processes, local climate effect, numerical simulation experiments

1. Introduction

Numerical models of mass and energy exchange in soil-vegetation-atmosphere continuum are of great important scientific sense and applicable values to the research of local or regional climate and global climate change. In the atmospheric surface layer, there are two basic exchange processes—hydrological circulation and thermal transportation, which directly influence local climate and environmental ecosystem. Only by carefully studying each detailed physical character of hydrological and thermal balance in soil, vegetation and atmosphere, together with the hydrological and thermal exchange at interfaces of soil-vegetation-atmosphere, can we clearly understand the effect of forest vegetation on local and regional climate impact and responses. In addition, forest vegetation has important effect on atmospheric boundary structure,

atmospheric circulation, etc. Deardorff (1978) first put forward the parameterization of land-atmosphere interaction, and Dickinson (1984, 1986) advanced a Biosphere-Atmosphere Transfer System (BATS) and modified it afterwards, while Sellers (1986) advanced a simple biosphere model (SiB). These studies have laid a foundation for the numerical simulation models of mass and energy exchange in soil-vegetation-atmosphere continuum.

Particular study on turbulent transportation in atmospheric canopy was first put forward by Yamada (1982), whose model was fit for non-neutral atmosphere. He expanded his study to the area over the plant canopy, and then attained the coupling of canopy and atmosphere. Although the model had some shortcomings, such as taking no account of hydrological transportation and incomplete consideration of turbulent airflow, his model still was of perfect

*Supported by the National Natural Science Foundation of China under Grant Nos. 40275004 and 49575251.

[†]Corresponding author E-mail: lshuhua@pku.edu.cn

representation. Raupach and Shaw (1982), Li et al. (1985, 1990), and Naot and Mahrer (1989) have advanced and developed vegetation micrometeorological models of their own, and have studied the rules of the mass, water vapor, and thermal exchange in canopy in different aspects. These studies are of great importance in the research of canopy micrometeorology, dynamical and thermodynamic transportation together with biological and chemical processes of the plant ecosystem, and the productivity of this system.

In recent years, with the development of the study of land surface processes, numerical simulation models, which regarded soil-vegetation-atmosphere system as a continuum, appeared in the research field of meteorology. Liu et al. (1996, 2002) have used a one-dimensional soil-vegetation-atmosphere coupled numerical simulation model to study the evaporation and transpiration processes in the atmospheric surface layer based on different vegetation coverage in summer in the arid and semiarid areas in the northwest of China, and moreover, they have done a series of sensitivity tests of interaction between land surface physical processes and atmospheric boundary layer. This paper will couple the atmospheric boundary layer and micrometeorological models in plant canopy, take some physical operations of vegetation in the transportation of radiation, momentum, and heat into consideration, and establish a numerical model of the mass and energy exchange in soil-vegetation-atmosphere continuum. Then, we will use this model to perform numerical simulation experiments of the diurnal variations of each physical factor's profile in the atmospheric boundary layer with forest underlying surfaces, the variation rules of canopy temperature, air temperature in canopy, and thermal fluxes at surfaces of leaves, the distribution of turbulence, temperature, and wind fields based on a non-homogeneous underlying surface, as well as its circulation character. The results of this simulation will help offset the shortage of realistic observations and enhance our understandings of mass and energy transportation processes in forest canopy and the influence of forest on local and regional climate.

2. Numerical model and parameterization

The basic equation sets and parameterization

schemes of land surface physical processes and atmospheric boundary layer model in this paper have already been described quite sufficiently in the studies by Liu et al. (2002). In this section, we only present the advancement done on the forest underlying surface.

2.1 Turbulence exchange coefficient

The evaluation of turbulence exchange coefficient has been put forward by many scholars of different models. In this paper, we adopt the scheme of Blackadar (1962) to calculate mixing length l , and then obtain momentum exchange coefficient K . The shear of wind speed S_w can be written as

$$S_w = \left(\left(\frac{\partial u}{\partial z} \right)^2 + \left(\frac{\partial w}{\partial z} \right)^2 \right)^{1/2}. \quad (1)$$

Given vegetation height as h_t , when $z > h_t$, the mixing length l has the form

$$l = \frac{k_0(z + z_0)}{1 + \frac{k_0(z + z_0)}{\beta}}, \quad (2)$$

where Karman constant $k_0=0.4$; z_0 is the surface roughness length; inside forest the vegetation coverage is assumed to be V_{eg} ; leaf area density (leaf area per unit volume) is $\mu(z)$ (here μ is a constant); β is the geostrophic parameter, and $\beta = \frac{27 \times 10^{-5} V_g}{f}$, while V_g is the geostrophic wind, and f is Coriolis parameter, $f = 2\omega \cos\varphi$, here ω is the geostrophic angular speed, and φ the geographical latitude. Then the form of mixing length is (see Wilson and Shaw, 1977)

$$l = \frac{0.03}{C_h \mu \cdot V_{eg}}. \quad (3)$$

A universal expression of K is (see Liu and Chen, 1993)

$$K = \begin{cases} l^2 S_w (1 + \alpha R_i) & R_i < 0 \\ l^2 S_w (1 - \alpha R_i) & R_i \geq 0, \end{cases} \quad (4)$$

where R_i is Richardson number, and can be written as

$$R_i = \frac{g}{\theta} \frac{\partial \theta / \partial z}{S_w^2}. \quad (5)$$

Here $\alpha=-3$ is a constant. In this model, $K_{mH} = K_{mV} = K$, $K_{qH} = K_{qV} = \alpha_p K$, $K_{\theta H} = K_{\theta V} = \alpha_p K$,

in which subscripts m, q and θ stand for momentum hydrologic and thermal exchange coefficients, and H and V denote the horizontal and vertical directions, respectively. α_p is the Prandtl reciprocal, and $\alpha_p=1.35$.

2.2 Radiation energy fluxes

2.2.1 Shortwave radiation energy

We assume that vegetation coverage is V_{eg} , leaf reflectivity is α_h , and neglect the absorption caused by photosynthesis of plants, then the direct shortwave radiation flux S_f used to produce thermal impact among S_{down} , which is absorbed by the top layer of vegetation is

$$S_f = V_{eg}(1 - \alpha_h)S_{down}. \quad (6)$$

When land surface albedo is α_g , the shortwave radiation flux of land surface thermal impact S_g is

$$S_g = (1 - V_{eg})(1 - \alpha_g)S_{down}, \quad (7)$$

where the thermal impact caused by reflective shortwave radiation of land surface and vegetation is ignored.

The direct shortwave radiation flux absorbed by the top layer of vegetation is (see Kondratyev, 1969)

$$S_{down} = (t - a)S_0 \cos Z, \quad (8)$$

where t is an empirical parameter given by Kondratyev (1969) after considering firmamental diffuse reflection; a is the absorption coefficient of atmosphere to solar spectrum (see Yamada, 1983); S_0 is the solar constant (1367 W m^{-2}); and Z is solar altitude angle.

2.2.2 Longwave radiation fluxes

According to Kondratyev (1969) the downward longwave radiation flux of atmosphere is

$$L_a = \varepsilon_a \sigma T_a^4, \quad (9)$$

where σ is the Stefan-Boltzmann constant, and $\sigma=5.68 \times 10^{-8} \text{ W m}^{-2} \text{ K}^{-4}$; T_a is the temperature of referenced atmospheric layer; ε_a is the atmospheric longwave emitting coefficient (see Liu et al., 2002). The longwave radiation flux of vegetation is

$$L_f = 2V_{eg} \cdot \varepsilon_f \sigma T_f^4, \quad (10)$$

where T_f is the (average) temperature of vegetation layer, and as the vertical distribution of vegetation temperature has not been taken into account in this model, T_f is merely a function of special position, and $x \cdot \varepsilon_f$ is the vegetation longwave emitting coefficient, and $\varepsilon_f=0.95$. Factor 2 represents a situation including both the upward radiation and downward radiation of vegetation. The longwave radiation flux of land surface is

$$L_g = \varepsilon_g \sigma T_{gs}^4, \quad (11)$$

where T_{gs} is the land surface temperature; ε_g is the land surface longwave emitting coefficient, taking as 0.91 in this paper.

Simplifying longwave absorption by assuming that longwave radiation can be absorbed completely by vegetation and land surface, and ignoring the reflection of longwave radiation, we can obtain the longwave absorption of vegetation layer (L_{fin}) and land surface (L_{gin}) as

$$L_{fin} = V_{eg} \cdot (L_a + L_g), \quad (12)$$

$$L_{gin} = (1 - V_{eg})L_a + \frac{1}{2}L_f. \quad (13)$$

2.2.3 Total radiation energy fluxes

The total radiation flux of vegetation is

$$R_{nf} = S_f + L_{fin} - L_f. \quad (14)$$

Similarly, the total radiation flux of land surface is

$$R_{ng} = S_g + L_{gin} - L_g. \quad (15)$$

2.3 Vegetation layer subsystem

2.3.1 Sensible heat flux of vegetation

The thermal flux transported to the atmosphere from per unit volume vegetation is

$$H_{fv}(x, z, t) = \begin{cases} V_{eg} \mu(z) \rho_a c_p (T_f(x) - T_a(x, z, t)) / R_a & z < h \\ 0 & z > h, \end{cases} \quad (16)$$

where subscript v denotes thermal flux per unit volume; ρ_a is the density of atmosphere, and R_a is the atmospheric dynamical resistance of leaf surface, and has the form

$$R_a = 1/[C_f u(x, z, t)], \quad (17)$$

where C_f is the momentum, thermal and hydrologic transportation coefficient of vegetation, and is decided by the formula underneath

$$C_f = 0.01 \left(1 + \frac{0.3}{u(x, z, t)} \right). \quad (18)$$

T_f is the temperature of plant canopy, which is a function of abscissa x .

The thermal source in atmospheric dynamical equation is

$$S_h = H_{fv}. \quad (19)$$

The total thermal flux per unit area canopy is

$$H_{fs}(x, t) = \int_0^h H_{fv}(x, z, t) dz, \quad (20)$$

where subscript s denotes unit area.

2.3.2 Latent heat flux of plant canopy

If we neglect the water intercepted by leaf surface, the calculating formula of the total transpiration of leaf surface is (see Noilhan and Planton, 1989)

$$E_{hv} = V_{eg} \mu(z) \rho_a \frac{q_{sat}(T_s) - q_a}{R_a + R_s}, \quad (21)$$

where $q_{sat}(T_s)$ is the saturated water vapor pressure at temperature T_s , while q_a is the water vapor pressure in the atmosphere; R_s is the surface resistance of vegetation system. The parameterization has been described in detail by Liu et al. (2002) and Noilhan and Planton (1989).

The total transpiration per unit area vegetation is

$$E_{hs} = \int_0^h E_{hv} dz. \quad (22)$$

In this way, the latent heat flux of vegetation can be written as λE_{hv} , where the vaporization heat of water is $\lambda = 2.5 \times 10^6 \text{ J kg}^{-1}$.

2.3.3 Vegetation temperature equation

Given expressions of sensible heat flux and latent heat flux of vegetation, we can write out the equation of vegetation temperature:

$$C_h \frac{\partial T_f}{\partial t} = R_{nf} - H_{fs} - \lambda E_{hs}, \quad (23)$$

where C_h is the thermal capacity per unit area vegetation and has the form

$$C_h = 0.02 I_{LA} C_w, \quad (24)$$

with I_{LA} being the leaf area index, and C_w the thermal capacity of water.

2.3.4 Other fluxes transported to atmosphere from vegetation

Similar to the written manner of thermal fluxes, the voluminal density of vegetation momentum flux can be written as

$$S_p = -V_{eg} \mu(z) \rho_a U(x, z, t) / R_a. \quad (25)$$

The voluminal density of hydrologic flux is

$$S_q = E_{hv}. \quad (26)$$

2.4 Soil subsystem

2.4.1 Physical quantity fluxes of soil and their connecting conditions with atmosphere

We will consider thermal and hydrologic transportation from land surface to atmosphere alone, and eliminate vegetation, thus we cannot use reference layer and atmospheric dynamical resistance scheme to calculate fluxes. Because the grid spacing of bottom layer is very small, we can consider that the thermal and hydrologic fluxes in this thin layer of atmosphere are those of land surface. The temperature and humidity at the bottom of this thin layer can only be decided by the characters of soil surface, and their fluxes can be calculated using temperature and water vapor gradients.

The equations of thermal flux transported from soil to the bottom of atmosphere can be written as

$$H_g = \rho_a c_p K_{\theta V} \frac{\partial T_a}{\partial z} \Big|_{z=0}, \quad (27)$$

$$T_a(0) = T_{gs} \Big|_{z=0}, \quad (28)$$

where $T_{gs}(0)$ and $T_a(0)$ represent soil temperature and atmospheric temperature at the height of zero, respectively, and their calculating schemes will be discussed hereinafter.

Similarly, the equations of energy and water vapor fluxes are

$$E_g = \rho_a K_{qv} \left. \frac{\partial Q_a}{\partial z} \right|_{z=0}, \quad (29)$$

$$Q_a(0) = h_u Q_{sat}(T_{gs}) \Big|_{z=0}, \quad (30)$$

where $Q_a(0)$ is the atmospheric humidity at the land surface height of zero; h_u is the relative humidity at land surface (see Noilhan and Planton, 1989); $Q_{sat}(T_s)$ is the saturated humidity when land surface temperature is T_s , which can be calculated using Teten equation (see Liu et al., 2002)

$$e_s(T_s) = 6.1 \exp\left(\frac{17.269 T_s - 273.16}{T_s - 35.86}\right), \quad (31)$$

$$Q_{sat}(T_s) = 0.622 \frac{e_s(T_s)}{p - 0.378 e_s(T_s)}. \quad (32)$$

To deal with land surface momentum flux and wind speed, we can assume $U(0)=0$. As a result, at the surface of soil, the connecting condition of temperature can be written as

$$C \left. \frac{\partial T_g}{\partial z} \right|_{z=0} = R_{ng} - H_g - \lambda E_g, \quad (33)$$

where T_g represents soil temperature.

2.4.2 Soil temperature equation

As this paper mainly studies temperature and humidity at land surface, we can adopt a two-dimensional continuous medium thermal conduction equation to calculate soil temperature, and neglect latent heat flux in soil. If we assume soil temperature to be $T_g(x, z, t)$, then

$$C_g \frac{\partial T_g}{\partial t} = \frac{\partial}{\partial x} \left\{ C \frac{\partial T_g}{\partial x} \right\} + \frac{\partial}{\partial z} \left\{ C \frac{\partial T_g}{\partial z} \right\}, \quad (34)$$

where C_g and C represent the thermal capacity per unit volume and thermal conduction efficiency of soil. Then we have

$$C_g = (1 + W_{sat})C_i + W_g C_w, \quad (35)$$

where W_{sat} is the saturated water capacity of soil; W_g is the water capacity of soil; and C_i is the thermal capacity per unit volume of dry soil. Their parameterizations are given by McCumber and Pielke (1981).

2.4.3 Surface layer temperature of soil

The surface layer temperature of soil can be decided implicitly by energy balance equation. In this

numerical model, we assume that the bottom layer of atmosphere is assigned by 0, the temperature of the layer assigned by k is $T_a(k)$, and the energy turbulent exchange coefficient is $K_{\theta V}(k)$. Then the difference expression is

$$K_{\theta V} \left. \frac{\partial T_a}{\partial z} \right|_{K=1} = K_{\theta V}(1) \frac{T_a(2) - T_a(0)}{z(2) - z(0)}. \quad (36)$$

For the part under the surface, we assume that the top layer is assigned by 0, and then the temperature of the layer assigned by k is $T_g(k)$, with the vertical coordinate $z_g(k)$

$$\left. \frac{\partial T_g}{\partial z} \right|_{K=1/2} = \frac{T_g(1) - T_a(0)}{z(1) - z(0)}, \quad (37)$$

$$T_a(0) = T_g(0) = T_{gs}. \quad (38)$$

Considering that the thermal flux in the thin layer of land surface does not vary with height, we can put difference expressions of each quantity into energy balance equation, and obtain the expression of T_{gs} .

$$T_{gs} = \left\{ R_{ng} + K_{\theta V}(1) c_p T_a(2) / [z(2) - z(0)] \right. \\ \left. - \lambda E_g + \alpha T_g / [z_g(1) - z_g(0)] \cdot K_{\theta V}(1) c_p \right\} \\ \left/ \left\{ (z(2) - z(0)) + \alpha / [z_g(1) - z_g(0)] \right\} \right. \quad (39)$$

2.4.4 Soil water capacity equation

In consideration of water capacity, this model cuts soil into two parts, that is, surface layer (0.01 m) and the layer below, which consists of root zone and gravitational infiltrating layer. Because of evaporation of water in the soil, the water capacity of surface layer has an obvious diurnal variation; whereas the water capacity of the layer below is steady correspondingly, and can fetch up the loss of water caused by the evaporation of surface layer and the pumping resulting from the transpiration of vegetation, thus the water capacity of forest soil mainly remains invariable. For the sake of making model simple, we will take water capacity of the layer below different typical vegetation styles as a constant W_g , and the water capacity of surface layer $W_{g0}(x, t)$ is a function of coordinate x and time t . With precipitation neglected, the equation of surface layer water capacity can be written as

(see Deardorff, 1978; Liu et al., 1998, 2002; Noilhan and Planton, 1989)

$$\frac{\partial W_{g0}}{\partial t} = -\frac{C_1}{\rho_w d_1} E_g - \frac{C_2}{\tau} (W_g - W_{geq})$$

$$0 \leq W_g \leq W_{sat}, \quad (40)$$

where ρ_w is the density of liquid water; E_g is the evaporation of soil water; W_{geq} is the volume water capacity of soil surface when gravity and capillarity tension are balanced (see McCumber and Pielke, 1981)

$$W_{geq} = W_g - a \left(\frac{W_g}{W_{sat}} \right)^p \left(1 - \frac{W_g}{W_{sat}} \right)^{8p} W_{sat}. \quad (41)$$

In Eq.(40), d_1 is the thickness of soil surface layer, which is 0.01 m; coefficients C_1 and C_2 can be calculated by the formulae below

$$C_1 = C_{1sat} \left(\frac{W_{sat}}{W_g} \right)^{\frac{b}{2}+1}, \quad (42)$$

$$C_2 = C_{2ref} \left(\frac{W_2}{W_{sat} - W_2 + W_{fl}} \right), \quad (43)$$

where W_{fl} is a tiny constant which makes the formula above reasonable when soil is saturated, and in this paper it is 0.05. $C_{1sat}=0.375$ and $C_{2ref}=0.3$.

3. Difference scheme, boundary conditions, and initial conditions

The area simulated by this model is a two-dimensional space having a length of 60 km, a width of 4 km, and a depth of 40 cm. We put this area into grids in order to do numerical calculation. The horizontal orientation is divided into 60 grids equally, while the vertical orientation is divided into 155 grids, where the vertical orientation of soil is divided into 10 grids equally, while that of atmosphere is divided into 145 grids unevenly: the first layer is divided into 50 grids, with a height extension of 0-82 m, containing a vegetation area of 25 m; the second layer is divided into 45 grids, with a height extension of 82-500 m; the third layer is divided into 25 grids, with a height extension of 500-1500 m; and the fourth layer is divided into 25 grids, with a height extension of 1500-4000 m.

The area simulated is larger than the actual area to be studied. The wind speed, potential temperature, humidity, and soil temperature of windward boundary are taken as averages of values of 3 neighboring

grids, while similarly the values of leeward boundary are taken as averages of values of 3 neighboring grids. We assume that the physical quantities at top boundary and their fluxes are constants, that is, values of the two layers at top boundary are invariable. The soil temperature of a certain depth at bottom boundary is constant. As the model simulates the variation of all values within 24 hours, the initial conditions should accord with the results of simulation after 24 hours, that is, they can sequentially become initial conditions of the next 24 hours. As a result of this consideration, for the sake of gaining reasonable initial conditions, we first prescribe a set of initial conditions factitiously according to practical experiences, and make the model run 24 hours. Then the final situations we obtain should be more suitable to be initial conditions. (This is because ecosystem has a rather powerful stability, and a steady semi-periodic estate has a certain kind of attrahent effect on neighboring orbits which have some windages, and will make them converge to the steady semi-periodic estate finally.) As a result, the scheme in this paper is to simulate values of some days continuously, abnegate the values of the first 24 hours, and just study the simulation results after the first 24 hours.

Initial wind speed (m s^{-1}) profile

$$u(i, k) = \begin{cases} 4.5 \left(\frac{z}{10.0} \right)^{0.14} & z < 1500 \text{ m} \\ u|_{z=1500 \text{ m}} & 1500 \text{ m} \leq z < 4000 \text{ m}. \end{cases} \quad (44)$$

Initial potential temperature (K) profile

$$\theta(i, k) = \begin{cases} 287.5 & 0 \leq z \leq 500 \text{ m} \\ 298.0 & 500 \text{ m} \leq z < 1000 \text{ m} \\ 298.0 + \frac{1.5(z-1000)}{100} & 1000 \text{ m} \leq z < 1500 \text{ m} \\ 305.5 + \frac{0.5(z-1500)}{100} & 1500 \text{ m} \leq z < 4000 \text{ m}. \end{cases} \quad (45)$$

Initial humidity (kg kg^{-1}) profile

$$Q(i, k) = 0.006 - 10^{-6} z. \quad (46)$$

Leaf surface temperature

$$T_f(i) = 290.0. \quad (47)$$

Initial soil water capacity ($\text{m}^3 \text{m}^{-3}$)

$$W_g(i) = 0.4, \quad W_2 = 0.4. \quad (48)$$

Soil temperature

$$T_{gs}(i) = T_g(i) = 290. \quad (49)$$

The time step of simulation is 1 s, and rhombic skipping scheme is adopted as difference format, which is steady state.

4. Simulation results and discussion

4.1 *Micrometeorological ecological environment characters of forest ecosystem*

The environment simulated in this paper is a middle-latitude area in early summer, and the latitude is located at 45.6°N while the beginning time is the 200th day of a calendar year, that is 19 July. Typical plant in this area is temperate broad-leaved forest and the characteristic parameters of vegetation and soil are given in Table 1, which are selected according to Wang et al. (1985).

Table 1. Characteristic parameters of soil and vegetation

Parameter	Value
Vegetation fraction (V_{eg})	0.8
Top of the canopy (h)	25 m
Leaf area index (I_{LA})	$0.4 \text{ m}^2 \text{ m}^{-2}$
Albedo of leaf (α_h)	0.2
Resistance of leaf transpiration (R)	$40\text{-}5000 \text{ s m}^{-1}$
Temperature of stomata opening (T_0)	298 K
Specific heat capacity of dry soil	$321 \text{ J kg}^{-1} \text{ K}^{-1}$
Density of dry soil	200 kg m^{-3}
Saturation soil moisture content (W_{sat})	0.472 kg kg^{-1}
Plant withered moisture content (W_{wil})	0.015 kg kg^{-1}

By considering income and outgo of system boundary energy, at the upper boundary energy input is in the form of solar short wave radiation and downward atmospheric long wave radiation, while output is in the form of ground long wave radiation and turbulence exchange at 4 km. Energy transfer through the outgoing bottom boundary is mainly in the form of soil heat flux and sensible heat flux, while input and output of energy through lateral boundaries is neglected,

which is assumed to be balanced through left and right lateral boundaries.

Figures 1 and 2 respectively depict the numerical simulation results of diurnal variations, during the four-day period, of micrometeorological ecological environment characters of vegetation canopy, vegetation and ground temperature, moisture content of canopy air, air saturation content, and relative humidity. Figure 1 shows after sunrise vegetation temperature arises more rapidly than canopy and ground temperatures

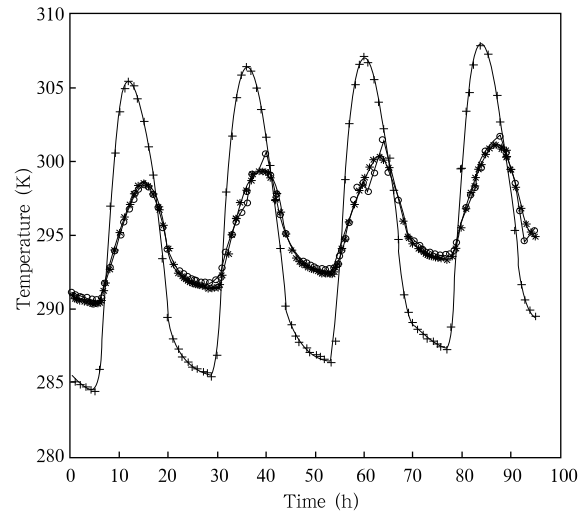


Fig.1. The numerical simulation results for diurnal variations of canopy temperature (asterisk), vegetation (bar), and ground surface temperature (circle).

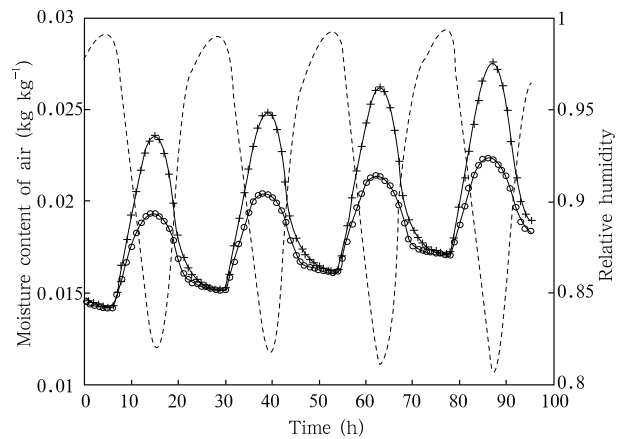


Fig.2. The numerical simulation results for diurnal variations of canopy air moisture content (bar), air saturation moisture content (circle), and relative humidity (dashed).

and reaches maximum value at 1200 LT (local time), because vegetation canopy absorbs and reserves solar radiation directly, which is consistent with diurnal variations of net radiation. But it reduces slower after reaching maximum due to heat storage of vegetation canopy, thus the pattern of diurnal variations is not normal distribution as net radiation flux is. The variation of vegetation canopy air temperature is coincident with that of ground temperature since the turbulence exchange within vegetation canopy layer is very weak. Figure 1 indicates that, in forest ecosystem, the solar radiation heats vegetation first, and then heats canopy air and ground, thus it is clear that vegetation canopy temperature rises faster than vegetation canopy air and ground temperatures, and the time of vegetation canopy temperature reaching maximum is earlier than the latter. At 1800 LT, canopy air temperature is equal to vegetation temperature and this time is called the constant atmospheric temperature point of vegetation canopy, and the sensible heat flux is zero at this time. Besides, we can see that from Fig.1, due to the accumulation of heat in forest ecosystem, temperatures of canopy air, vegetation, and ground increase day by day during the four-day period.

Figure 2 shows numerical simulation results of diurnal variations of canopy moisture content, saturation content, and relative humidity during four-day period. We can see that the variations of canopy moisture content and saturation moisture content are in accordance, while the variation of relative humidity is out of phase and this shows adequately their physical feature. With the increase of canopy air, vegetation, and ground temperatures, canopy moisture content, saturation moisture content, and relative humidity increase gradually, and this phenomenon also reflects the micrometeorological and ecological features of forest ecosystem.

4.2 Sensitivity experiments of land surface process, interaction between atmospheric boundary layer and local climate effects on non-uniform forest underlying surface

In order to examine the sensitivity of this model to land surface process, interaction between atmospheric boundary layer and local climate effects over

different underlying surfaces, we have conducted sensitivity experiment on parameters first and find that the percentage covered by vegetation and soil moisture content are more sensible. Subsequently, we will give the results of sensitivity experiments mentioned above. The bounding surface of two different underlying surfaces A and B is designed in the middle point of horizontal area in the model, that is at 30 km. Percentage covered by vegetation and soil moisture content of A and B are individually 0.8, 0.5 and 0.4, 0.3 (kg kg^{-1}).

Figure 3 shows diurnal variations of ground and canopy air temperatures at horizontal grid located at 14400 and 44400 m for A and B, which are two different underlying surfaces. We can see that air temperature difference in canopy over underlying surface A is 10 K, and daily average temperature is also 296 K, while the air temperature difference in canopy of underlying surface B is 12 K, and daily average temperature is about 297 K, it has 2 K fluctuation more than that over A. The variation range of ground temperature of B is more broad than that of A (8 K). This phenomenon indicates that ground and vegetation over underlying surfaces A and B heat their surface air in different means. At area with higher percentage covered by vegetation, the vegetation is the

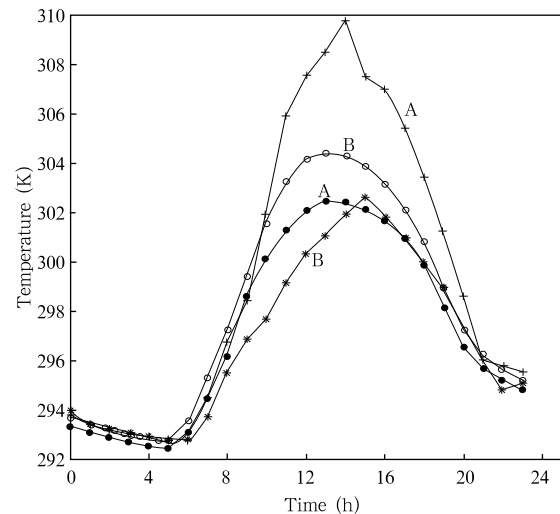


Fig.3. Comparisons of diurnal variations of ground surface temperature(dot,circle) and canopy air temperature(cross,asterisk) over underlying surfaces A and B.

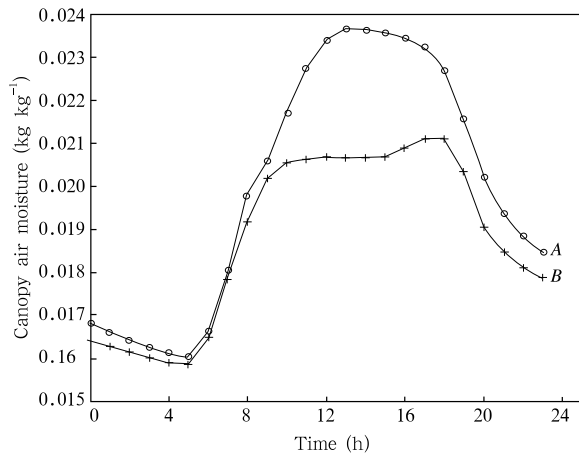


Fig.4. Comparisons of diurnal variations of canopy moisture content over underlying surfaces A(circle) and B(cross).

main source of heat, and ground is the main source of heat in other cases. Canopy converts energy of short-wave radiation into latent heat by transpiration in daytime, thus it could keep lower temperature, while lower percentage covered by vegetation only keep the total energy balance one day by increasing long wave radiation and sensible heat. At night time, transpiration of vegetation diminishes, hence the difference of underlying surfaces A and B is not obvious and temperature is gradually driven to the same by the effect of horizontal wind.

Figure 4 shows patterns of diurnal variations of canopy air specific humidity under two vegetation percentages of coverage. Transpiration of A and B is different due to the different distribution of vegetation percentage, which leads to the difference of air specific humidity in canopy at daytime. A point which should be paid attention to is that air specific humidity experiences a small rebound over underlying surface B at 1700 LT, and at this time B is leeward, which means there is a humidity gradient down the wind, thus the variation of specific humidity of B includes moisture horizontally transported from A. With the limit of wind speed, the variation of moisture transported from A is delayed compared with that of A itself, and that means there is time lag. The water vapor transfer from A can also explain the rebound of

air moisture content over B at 1700 LT.

The non-uniform spatial distribution of physical characters of underlying vegetation surface will exert effects on land surface physical process, atmospheric boundary layer, and local climate effects, therefore we analyze space distribution features of simulation results of temperature, turbulence intensity, wind speed, and specific humidity.

Figure 5 shows temporal and spatial distributions of potential temperature over nonhomogeneous underlying surfaces. From temporal and spatial distributions of potential temperature at 0300 LT in Fig.5, we can see that the surface layer is stable and the temporal and spatial distributions of potential temperature are uniform. With the increase of solar radiant energy received by land surface after sunrise, the difference of vegetation cover percentage and soil moisture content leads to further difference of thermal features and affects the distribution of temperature in atmospheric boundary layer. Because percentage of vegetation coverage of underlying surface B is relatively small, the energy consumption by transpiration of plants is less than that over underlying surface A in daytime, and the heating of ground surface layer makes its temperature higher than that over underlying surface A, which has larger sensible heat flux and longwave radiation to balance solar shortwave radiation. We can see this point from the figure of 5 temporal and spatial distributions of potential temperature at 0600, 0900, 1200, 1500, and 1800 LT. Accompanied with the cooling of ground surface and atmosphere layer after sunset, isothermal lines tend to flat fast for the movement of atmosphere. Nonhomogeneity of underlying surface A and B leads to the nonhomogeneity of transport of heat and momentum, which would affect the dynamic and thermal features of atmospheric boundary layer, including turbulence movement, the formation of atmospheric circulation etc.

From temporal and spatial distribution patterns of turbulence exchange coefficient shown in Fig.6, we can see the formation process of eddy over underlying surfaces A and B. After sunrise, canopy temperature increase over underlying surface B is faster than that

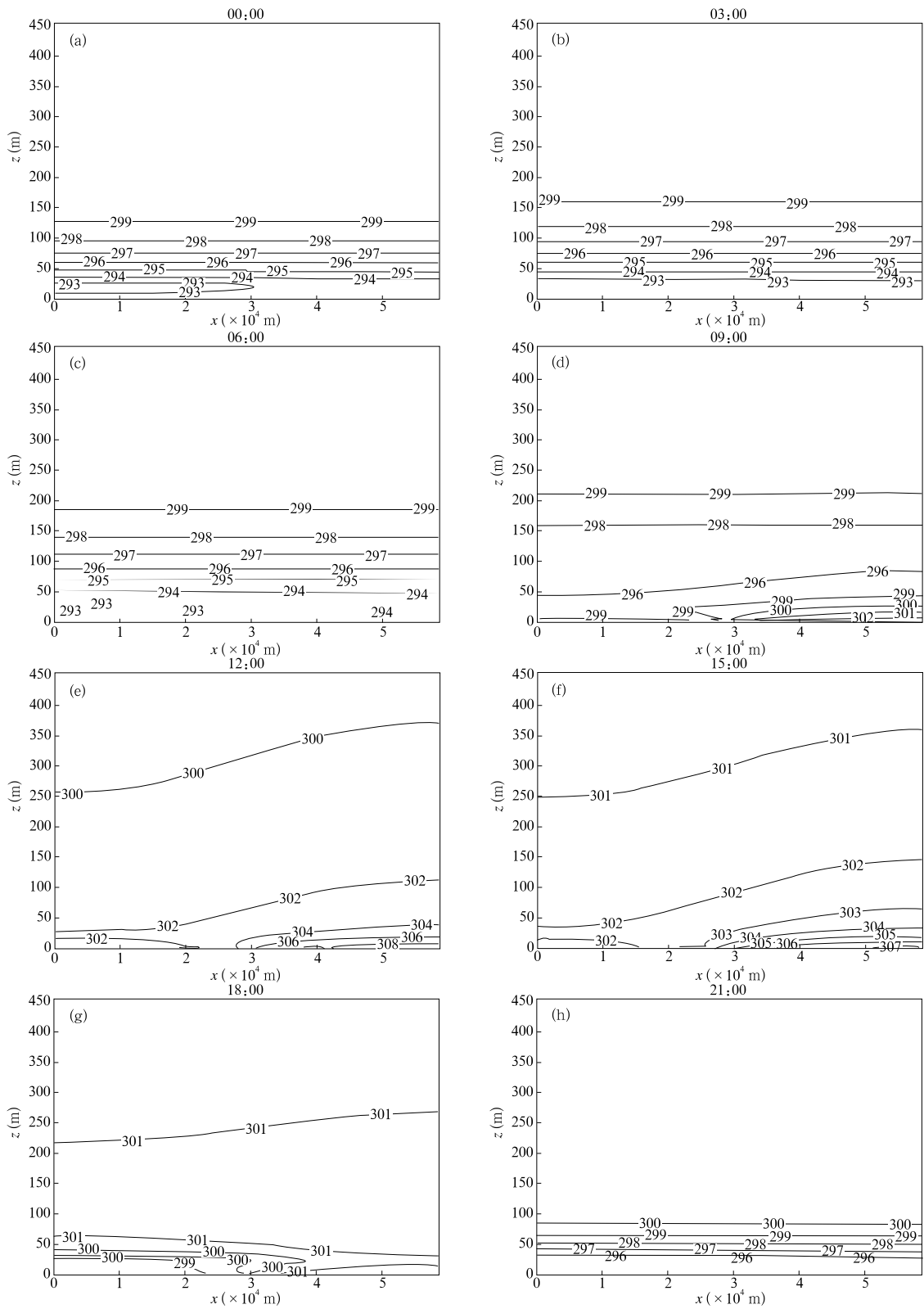


Fig.5. Temporal and spatial distributions of potential temperature (K) over nonhomogeneous underlying surfaces. (a) 00:00, (b) 03:00, (c) 06:00, (d) 09:00, (e) 12:00, (f) 15:00, (g) 18:00, and (h)21:00.

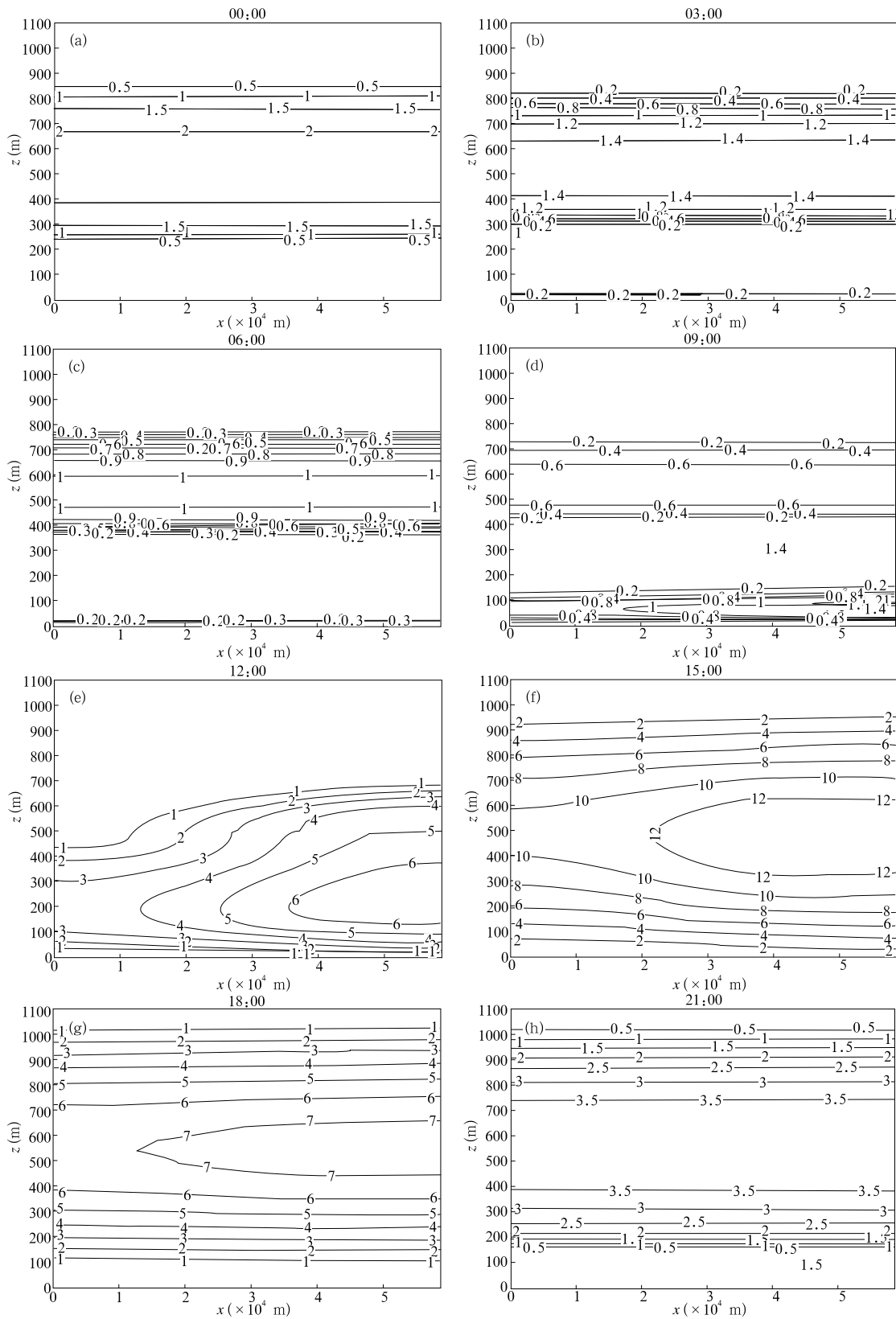


Fig. 6. Temporal and spatial distributions of turbulence exchange coefficient ($\text{m}^2 \text{s}^{-1}$) over nonhomogeneous underlying surfaces. (a) 00:00, (b) 03:00, (c) 06:00, (d) 09:00, (e) 12:00, (f) 15:00, (g) 18:00, and (h) 21:00.

over A, thus turbulence activity is strengthened and eddies arise first in B. For all daytime, turbulence activity over underlying surface B at certain height is stronger than that over A. Turbulence activity declines rapidly about after sunset, while eddy activity at the height of 500 m will maintain active until midnight. We can see clearly from Fig.6 the effect of underlying surface on atmospheric turbulence transport. Nonhomogeneity of spatial distribution of temperature and turbulence exchange coefficients will lead to the formation of vertical air flow which is an important factor for the formation of local climate feature, and in the following we will show temporal and spatial distributions of vertical wind.

Figure 7 gives only temporal and spatial distributions of vertical wind at 0000, 0600, 1200, and 1800 LT, for a clearer pattern. Vertical wind over underly-

ing surface A is negative in general (downwards), while vertical wind over underlying surface B is positive (upwards). Besides, the difference of ground temperature of underlying surfaces A and B with different percentage of coverage leads to the generation of horizontal pressure gradient, which is the direct reason for the formation of local atmospheric circulation in daytime. With the homogeneous tendency of underlying surface temperature at dusk, pressure gradient becomes weak, so does the circulation. Atmosphere circulation will reverse at night for the heat storage of vegetation and longwave radiation effect.

Features of heat, momentum, and circulation of surface layer and atmospheric boundary layer over different vegetation coverage underlying surfaces would cause the transfer of moisture and the variation of moisture field certainly. Figure 8 shows the spatial

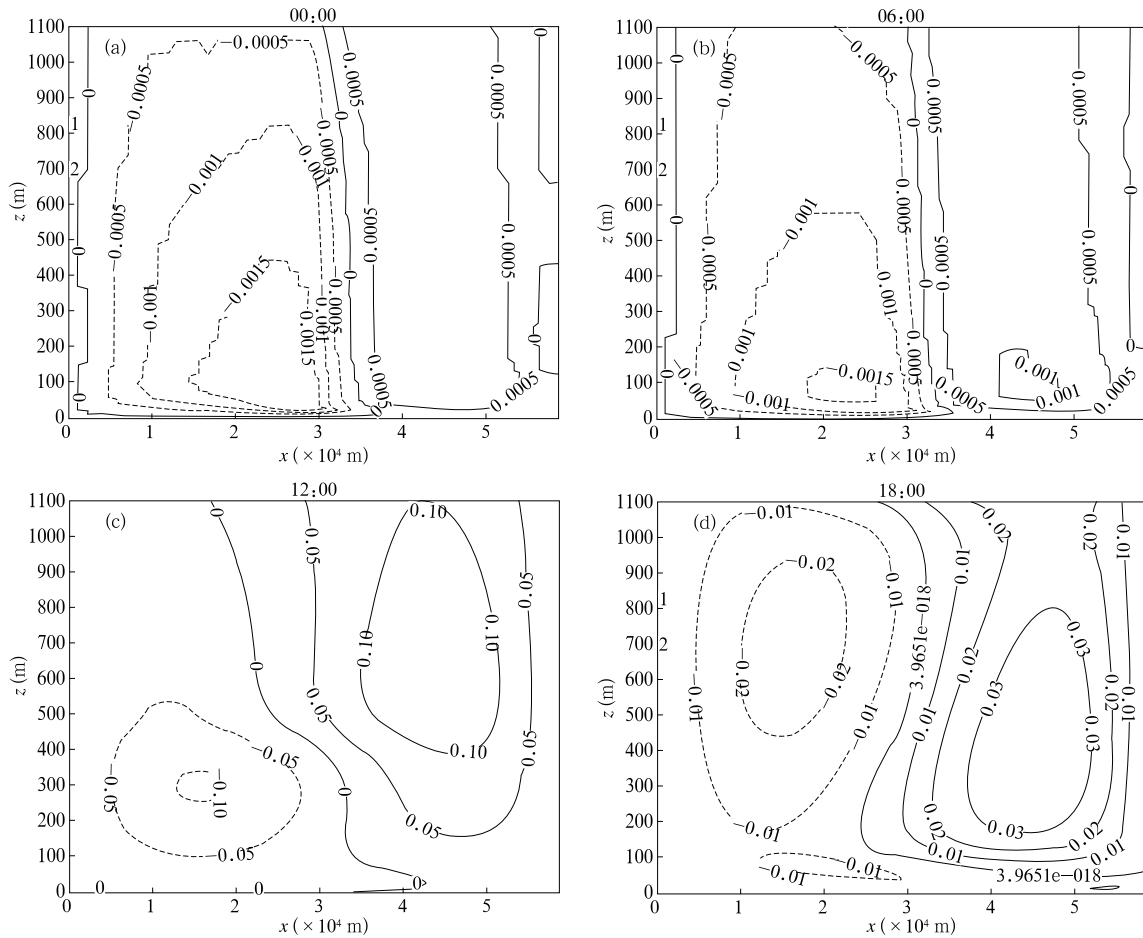


Fig.7. Temporal and spatial distributions of vertical wind velocity (m s^{-1}) over nonhomogeneous underlying surfaces. (a) 00:00, (b) 06:00, (c) 12:00, and (d) 18:00.

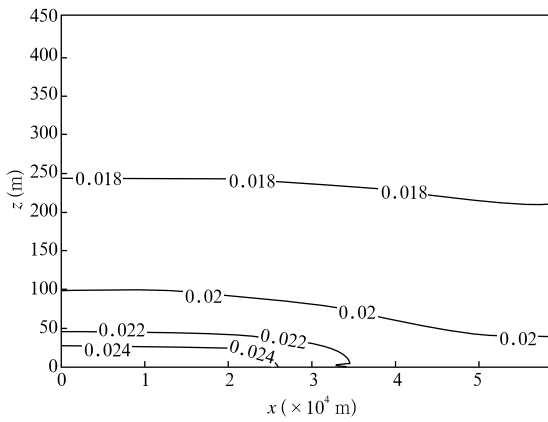


Fig.8. Temporal and spatial distributions of air moisture content (kg kg^{-1}) over nonhomogeneous underlying surfaces.

distribution of air moisture content over different underlying surfaces at 1400 LT, from which we can see that air humidity over underlying surface A is obviously higher than that over underlying surface B at the same height, and this incarnates the important contribution area of vegetation canopy to surface layer moisture content as well as the local climate and ecological environment effects. Because vegetation transpiration almost stops at night, the distribution of air specific humidity tends to be homogeneous again due to the movement of atmosphere (figure omitted).

5. Conclusions and discussions

Based on basic principles of atmospheric boundary layer and plant canopy micrometeorology, a physical process model of land surface with forest underlying surface and a two-dimensional numerical model of atmospheric boundary layer have been developed and numerical simulation experiments of biosphere and physiological process of vegetation and soil volumetric water content have been carried out on land surface process with local climate effect. In order to examine the sensitivity of basic parameters of model to land surface physical process, interaction between atmospheric boundary layer and local climate effect, we have conducted some sensible experiments on the vegetation percentage of coverage and soil moisture content. The numerical simulation results show agreement with experience, which can be used to obtain

reasonable simulation for diurnal variations of canopy temperature, air temperature in canopy, ground surface temperature, and temporal and spatial distributions and diurnal variations of potential temperature, vertical wind velocity, relative humidity, and turbulence exchange coefficient over the atmospheric boundary layer with forest underlying surface.

The model developed in this paper has simplified the varying processes of some physical quantities, and the choice of parameters also has great adjusting space. We take the distribution of vegetation leaf area index as a very simple function of plant height, and assume that vegetation temperature is equally the same at every height in vegetation. Moreover, we have not taken the distribution of radiation intensity in vegetation into account, but only simply consider that radiation energy disperses equally at every height of canopy. The expressions of these simplifications have great differences with reality, and require theoretic improvement using further practical observations. For instance, we should develop reasonable formulae of leaf area index distribution, radiation index distribution in vegetation, etc., so as to enable the model to simulate mass and energy exchange processes in soil-vegetation-atmosphere continuum as well as the mechanism of interactions between forest ecosystem and atmospheric boundary layer more accurately.

REFERENCES

- Blackadar, A. K., 1962: The vertical distribution of wind and turbulent exchange in a neutral atmosphere. *J. Geophys. Res.*, **67**, 3095-3102.
- Deardorff, J. W., 1978: Efficient prediction of ground surface temperature and moisture with inclusion of a layer of vegetation. *J. Geophys. Res.*, **83**, 1889-1903.
- Dickinson, R. E., 1986: Biosphere-Atmosphere Transfer Scheme (BATS) for the NCAR community climate model. NCAR/TN-275+STR.
- Dickinson, R. E., 1984: Modeling evapotranspiration for three-dimensional global climate models. *Climate Process and Climate Sensitivity*. J. E. Hanson and T. Takahashi, Eds., Geophys. Monogor. Amer. Geophys. Union, **29**, 58-72.
- Kondratyev, J., 1969: *Radiation in the Atmosphere*. Academic Press, New York.
- Li Z. J., Lin J. D., and Miller D. R., 1990: Air flow over and through a forest edge: A Steadystate numerical

- simulation. *Boundary-Layer Meteor.*, **51**, 179-197.
- Li Z. J., Miller D. R., and Lin J. D., 1985: A first-order closure scheme to describe countergradient momentum transport in plant canopies. *Boundary-Layer Meteor.*, **33**, 77-83.
- Liu Shuhua and Chen Hesheng, 1993: *Numerical simulation of atmospheric boundary layer of Gobi Desert, The Annual Shapotou desert experimental research station Lanzhou institute of desert research*, Lanzhou, Gansu Publishing House of Science and Technology, 27-36. (in Chinese)
- Liu Shuhua, Huang Zichen, and Liu Lichao, 1996: Numerical simulation of the evapotranspiration process in the soil-vegetation-atmosphere continuum. *Acta Geographica Sinica*, **51**(2), 118-125. (in Chinese)
- Liu Shuhua, Liu Heping, Li Sen, and Liu Lichao, 1998: A modified SiB model of biosphere-atmosphere transfer scheme. *Journal of Desert Research*, **18** (Supp.4), 7-16.
- Liu Shuhua, Wen Pinghui, Zhang Yunyan et al., 2002: Sensitivity tests of interaction between land surface physical process and atmospheric boundary layer, *Acta Meteorologica Sinica*, **16** (4), 451-469.
- McCumber, M. C., and R. A. Pielke, 1981: Simulation of the effects of surface fluxes of heat and moisture in a mesoscale numerical model, Part I. *J. Geophys. Res.*, **86**, 9929-9938.
- Naot, O., and Mahrer Y., 1989: Modeling microclimate environments: A verification study. *Boundary-Layer Meteor.*, **46**, 333-354.
- Noilhan, J., and S. Planton, 1989: A simple parameterization of land surface process for meteorological models. *Mon. Wea. Rev.*, **117**, 536-549.
- Raupach, M. R., and R. H. Shaw, 1982: Averaging procedures for flow within vegetation canopies. *Boundary-Layer Meteor.*, **22**, 79-90.
- Sellers, P. J., Z. Mintz, Y. C. Sud, and A. Dalcher, 1986: A simple model (SiB) for use within general circulation models. *J. Atmos. Sci.*, **43**, 505-531.
- Wang Zhengfei, Zhu Tingyao and Cui Qiwu, 1985: *Forest Meteorology*. Publishing House of China Forestry, Beijing, 507 pp. (in Chinese)
- Wilson, N. R., and R. H. Shaw, 1977: A high order closure model for canopy flow. *J. Appl. Meteor.*, **16**, 1197-1205.
- Yamada, T., 1982: A numerical model study of turbulent airflow in and above a forest canopy. *J. Meteor. Soc. Japan*, **60**, 439-455.
- Yamada, T., 1983: Simulations of nocturnal drainage flows by a q^2 -L turbulence closure model. *J. Atmos. Sci.*, **40**, 91-106.